Journal of Applied Physics ARTICLE scitation.org/journal/jap

Surface recombination velocities for 4H-SiC: Temperature dependence and difference in conductivity type at several crystal faces

Cite as: J. Appl. Phys. **127**, 195702 (2020); doi: 10.1063/5.0007900
Submitted: 17 March 2020 · Accepted: 3 May 2020 ·
Published Online: 15 May 2020

Masashi Kato,[1,2,a)] Zhang Xinchi,[1] Kimihiro Kohama,[1] Shuhei Fukaya,[1] and Masaya Ichimura[1]

AFFILIATIONS

[1]Department of Electric and Mechanical Engineering, Nagoya Institute of Technology, Nagoya 466-8555, Japan
[2]Frontier Research Institute for Materials Science, Nagoya Institute of Technology, Nagoya 466-8555, Japan

[a)]**Author to whom correspondence should be addressed:** kato.masashi@nitech.ac.jp

ABSTRACT

In bipolar SiC devices, which are promising under ultra-high voltage operation, the carrier lifetime is a highly influential parameter for the device performance. Surface recombination is one of the limiting factors for the carrier lifetime, and quantitative values of the surface recombination velocities are required for the design and development of fabrication processes of the devices. In this study, we observe carrier recombination at various temperatures for the Si- and C-faces of n- and p-type 4H-SiC samples and the *a*- and *m*-faces of n-type 4H-SiC samples with a treatment of chemical mechanical polishing or reactive ion etching by using the microwave photoconductivity decay method. From the experimental results, we estimate surface recombination velocities and bulk carrier lifetimes of the samples by using an analytical model. As a result, we found the smallest surface recombination velocity of 150 cm/s for the chemical mechanical polished surface of the Si-face of the n-type samples at room temperature. Surface recombination velocities increased with temperature for the chemical mechanical polished surfaces. The surfaces treated with reactive ion etching showed relatively large surface recombination velocities with weak temperature dependence. Based on these results, we discuss the origins of the recombination centers at surfaces of 4H-SiC.

INTRODUCTION

Silicon carbide (SiC) has a much higher breakdown electric field and a comparable electron mobility with Si. Power devices fabricated from SiC exhibit lower on-resistance and higher breakdown voltage than Si devices. In particular, at voltages higher than 10 kV, it is difficult to operate Si devices, and even for SiC devices, it is difficult to operate unipolar devices.[1,2] Therefore, bipolar SiC devices are promising because of low on-resistance owing to the conductivity modulation.[1–7] There have been a large number of reports on the fabrication of bipolar SiC devices. However, there are several difficulties to be overcome in the development of bipolar SiC devices, such as suppression of degradation and improvement of fabrication techniques for pn junctions. One of the important difficulties is the control of the carrier lifetime. The carrier lifetime directly affects the conductivity modulation behavior; thus, on-resistance and switching loss of the devices depend on the carrier lifetime.

Generally, the carrier lifetime in semiconductors is limited by Shockley Read Hall (SRH) recombination, bimolecular recombination, Auger recombination, and surface recombination. Among these factors, SRH recombination and surface recombination can be controlled by the crystal growth or surface treatment processes. Measurement results for SRH and surface recombination have been reported, and control processes for them have also been suggested in the literature.[8–26] Although the surface recombination velocity S for 4H-SiC has been reported by several groups so far, the reported surface recombination velocities are only for the Si- and C-faces,[15–24] or the processed surface of devices.[25,26] As seen in Refs. 25 and 26, bipolar devices frequently expose surfaces other than Si- and C-faces, and thus evaluation of surface recombination velocities for the various crystal faces is important for the design of the devices. In addition, temperature dependence of S has rarely been reported,[16] even though the SiC devices are expected to be operated at high temperatures. Therefore, accurate quantitative evaluation of S for various crystal faces including

temperature dependence is required for use in the design and fabrication processes of bipolar devices.

There are several techniques to observe carrier recombination.[8] Among them, the microwave photoconductivity decay (μ-PCD) method is highly sensitive and accurate for the detection of recombination of excited carriers in the low-injection condition.[27–29] Time-resolved photoluminescence (TR-PL) is also a sensitive technique for the observation of carrier recombination. TR-PL, however, sometimes includes signals from the recombination of stacking faults or dislocations,[30] and the signal component due to such defects overlaps with signals from surface recombination. Therefore, in this study, we adopted μ-PCD with improvement of time resolution compared with our previous study.[21,22] We have estimated S for the various crystal faces of n-type 4H-SiC and for the Si- and C-faces of p-type 4H-SiC.

EXPERIMENTS

Samples used in this work were free-standing n- and p-type 4H-SiC epilayers that were originally grown ∼150 μm thick on the (0001) Si-face with a 4° off-angle toward $\langle 11\bar{2}0\rangle$ of bulk single crystal 4H-SiC substrates. We also prepared ∼150 μm thick epilayers on the (1120) face (*a*-face) or the (1100) face (*m*-face) of 4H-SiC substrates, and these two epilayers were grown in the same batch. The N-doped n-type epilayers had a net donor concentration of 1×10^{15} cm^{-3}, but the *m*-face sample had unintentionally high net donor concentration of 1×10^{16} cm^{-3} even in the same growth batch with the *a*-face sample. The Al-doped p-type epilayers had a net acceptor concentration of 6×10^{14} cm^{-3}. The substrates for all the epilayers were completely polished, and both the front and back surfaces of the epilayers were treated by chemical mechanical polishing (CMP), which was performed by a commercial supplier of the polishing service. Then, the epilayers were cut into several pieces and prepared with several thicknesses for experiments to obtain the thickness dependence of the carrier recombination.[21,22] Pieces with three different thicknesses are considered as one set of samples. For a set of samples of each epilayer, we performed reactive ion etching (RIE) in SF_6+O_2 under a pressure of 20 Pa with 150 W for 30 min. In the case of the samples with the Si- and C-faces, we performed RIE for the Si- or C-face, whereas for the samples with *a*- and *m*-faces, we performed it for both sides of the *a*- and *m*-faces. The n-type Si- and C-face samples are the same samples as in our previous report.[21]

Carrier lifetimes for all the samples were measured by the μ-PCD method.[27] In the μ-PCD method, we employed 266 nm or 355 nm pulsed yttrium aluminum garnet (YAG) lasers with a pulse width of 1 ns as the excitation source. The penetration depths for 4H-SiC at room temperature are 1.2 μm and 42 μm for 266 nm and 355 nm, respectively,[31,32] and 1.2 μm penetration for 266 nm excitation makes surface recombination dominant in measured carrier lifetimes.[21–23] The samples were irradiated with microwaves of 10 GHz and their reflection was used as a probe. We measured the carrier lifetime with injected photon densities of 2×10^{13} cm^{-2} to keep the low-injection condition for reliable measurements with a sufficient signal to noise ratio.[28,29] Temperature of the samples was controlled from room temperature to 250 °C by hot air from a 3 kW heater with a temperature regulator. In addition, we have improved the time resolution of our μ-PCD system with better matching of impedance among a microwave detection diode, an amplifier, and an oscilloscope compared with the system in our previous reports for the estimation of surface recombination velocities[21,22] (the present system has already employed in our recent report for the characterization of surface passivation of SiC[23]). Time resolution of our present system is ∼2 ns.

NUMERICAL ANALYSIS

For the estimation of the surface recombination velocity S, we compared 1/e lifetimes $\tau_{1/e}$ (decay time from a peak to 1/e) obtained from experimental decay curves with numerically calculated curves. The following continuity equation was solved to obtain the excess carrier concentration $\Delta n(x, t)$ at given time t and depth x in a semiconductor layer,

$$\frac{\partial \Delta n(x,\,t)}{\partial t} = D_a \frac{\partial^2 \Delta n(x,\,t)}{\partial x^2} - \frac{\Delta n(x,\ t)}{\tau_{\rm epi}} - B\Delta n^2 - C\Delta n^3 + G, \quad (1)$$

where $\tau_{\rm epi}$ is the bulk carrier lifetime in the epilayers, D_a is the ambipolar diffusion coefficient, B is the radiation recombination coefficient, C is the Auger recombination coefficient, and G is the generation rate of the excess carriers. We adopted B of 2×10^{-14} cm^3 s^{-1} and C of 5×10^{-31} cm^6 s^{-1},[33] even though they are not significant in the low-injection condition, while we placed $G=0$ because of the absence of any excitation sources except for the initial laser pulse. The value of D_a was obtained from the following equation shown in Ref. 34,

$$D_a = \frac{p+n}{p/D_{\rm n} + n/D_{\rm p}}, \quad (2)$$

where n is the free electron concentration, p is the free hole concentration, and $D_{\rm n}$ and $D_{\rm p}$ are the diffusion constants of holes and electrons, which are estimated from the mobilities of electrons and holes $\mu_{\rm e}$ and $\mu_{\rm h}$, respectively. As the excess carrier concentration increases, $\mu_{\rm e}$ and $\mu_{\rm h}$ change due to the influence of electron–hole scattering.[28] The temperature dependence of $\mu_{\rm e}$ and $\mu_{\rm h}$ was extracted from the reported results, and anisotropy in $\mu_{\rm e}$ was considered.[1] Thus, $D_{\rm n}$ and $D_{\rm p}$ depend on excess carrier concentration, crystal face, and temperature, so D_a also depends on these factors through Eq. (2).

Boundary conditions at the excited and the other surfaces are given by

$$\begin{aligned} D_a \frac{\partial \Delta n(0,\ t)}{\partial x} &= S_0 \Delta n(0,\ t) \quad \text{and} \\ D_a \frac{\partial \Delta n(W,\ t)}{\partial x} &= -S_{\rm W} \Delta n(W,\ t), \end{aligned} \quad (3)$$

where S_0 and $S_{\rm W}$ are surface recombination velocities at the excited and other surfaces, respectively, and W is the thickness of the layer. In the case of analyses for the *a*- and *m*-face samples, S_0 and $S_{\rm W}$ were set to the same values.

The initial carrier concentration profile with illumination by a light pulse is expressed as

$$\Delta n(x, 0) = g_0 \exp(-\alpha x), \quad (4)$$

where g_0 is the carrier concentration at t = 0 and α is the absorption coefficient for the excitation wavelength. Temperature dependence of α is also included.[31]

From the solution of Eq. (1) using D_a from Eq. (2) and boundary conditions of Eq. (3) with the initial condition of Eq. (4), we calculated time-dependent μ-PCD signals from depth integration of the product of excess carrier concentrations and mobilities. In this work, we directly solved this partial differential equation using the method in Ref. 23, which is unlike the method of our other previous reports,[21,22] for improved validity of calculation. Then, S was estimated by fitting of $\tau_{1/e}$ obtained from experimental and calculated decay curves. Fitting was performed to minimize the sum of the relative error between the calculated and experimental $\tau_{1/e}$ in all measurement conditions with S_0, S_w, and τ_{epi} as parameters.

RESULTS

Figure 1 shows μ-PCD decay curves at room temperature for the CMP-treated C-face of n-type 4H-SiC excited by 266 nm, which is the measurement condition most sensitive to the surface recombination at the excited surface. Experimental $\tau_{1/e}$ extracted from these results are 0.19–0.27 μs, which is shorter than in our previous reports[21,22] due to better time resolution with a sufficient signal to noise ratio. At elapsed times after $\tau_{1/e}$, the slopes of the decay curves depend on the sample thickness, and the thicker samples show more gradual decay. This implies that the surface recombination at the non-excited surface (the Si-face) influences the decay curves due to the diffusion of the excited carriers. Thus, we consider that adoption of $\tau_{1/e}$ for fitting with the calculations is adequate to separate S between the excited and non-excited surfaces. We also performed the same measurement on the Si-face of the samples and also performed measurements with 355 nm excitation, and then extracted experimental $\tau_{1/e}$.

We plotted the experimental $\tau_{1/e}$ against the sample thickness for the n-type CMP-treated Si- and C-face samples at room temperature as shown in Fig. 2. For 355 nm excitation, $\tau_{1/e}$ is larger than those for 266 nm excitation and increases with thickness. In addition, $\tau_{1/e}$ for the Si-face excitation is larger than those for the C-face excitation. These tendencies are the same as in our previous reports.[21,22] The fitting with calculated $\tau_{1/e}$ results in $\tau_{epi} = 6\,\mu$s, S for the Si-face $S_{Si} = 150$ cm/s, and S for the C-face $S_C = 500$ cm/s. The lines in Fig. 2 indicate calculated $\tau_{1/e}$ using these values. The reproduced decay curves from the calculation are also shown in Fig. 1. In Fig. 1, there are some differences between the experiment and calculated decay curves, and in Fig. 2, for the case of the Si-face excited by 266 nm, there is a difference between experimental and calculated $\tau_{1/e}$. We consider that these differences originate from the experimental errors, but our analysis was successful to minimize the errors in estimation of S by using the measurements with various conditions as described later.

From the fitting results for all the measurement temperatures, we estimated the temperature dependence of S_{Si} and S_C for the n-type samples as shown in Fig. 3. In Fig. 3, we also show S obtained from the RIE-treated samples (but not S for the non-RIE-treated surface of the RIE-treated samples, because they are almost the same as those for the CMP-treated surfaces). S_C are larger than S_{Si}, and S of both faces for the RIE-treated surfaces are larger than those for the CMP-treated surfaces, as in previous reports.[22] S increases with temperature monotonically for the CMP-treated surfaces from 150 cm/s to 800 cm/s for the Si-face and from 500 cm/s to 1500 cm/s for the C-face. For the RIE-treated surface, S also increase with temperature in the ranges of

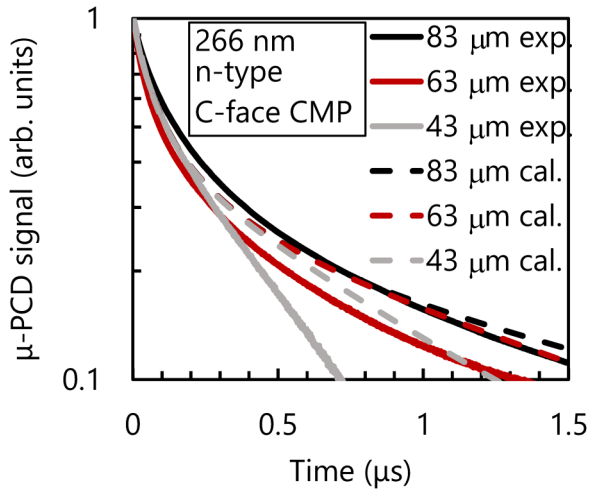

FIG. 1. μ-PCD decay curves for the CMP-treated C-face of the n-type 4H-SiC excited by 266 nm at room temperature. The solid lines are experimental curves at three epilayer thicknesses (43 μm, 63 μm, and 83 μm), and the dotted lines are calculated ones with $\tau_{epi} = 6\,\mu$s, $S_{Si} = 150$ cm/s, and $S_C = 500$ cm/s for the same three thicknesses.

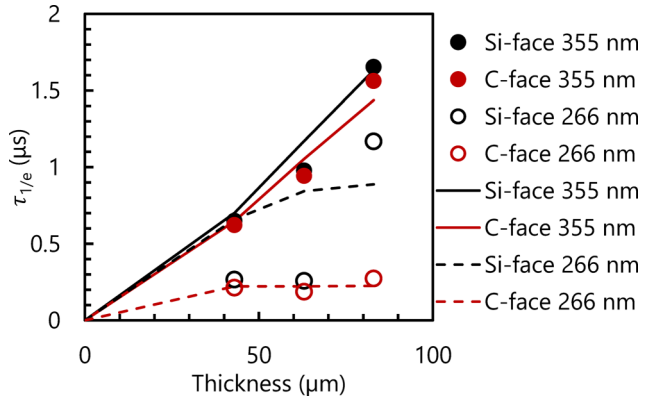

FIG. 2. The experimental (symbols) and calculated (lines) $\tau_{1/e}$ for the n-type CMP-treated Si- and C-face samples at room temperature. The calculated $\tau_{1/e}$ employs $\tau_{epi} = 6\,\mu$s, $S_{Si} = 150$ cm/s, and $S_C = 500$ cm/s.

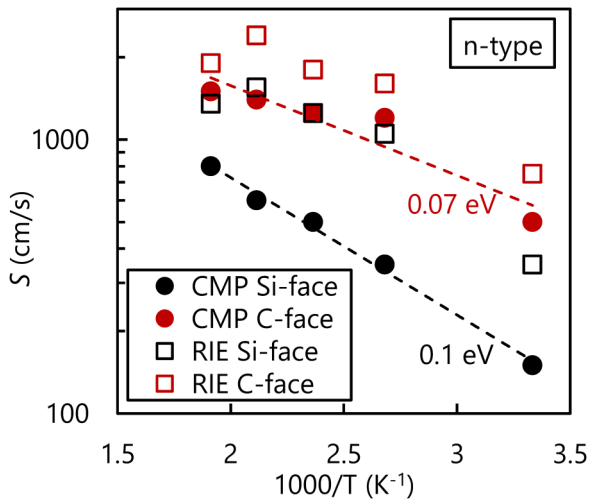

FIG. 3. Temperature dependence of S_{Si} and S_C for the n-type samples. The dotted lines are the slopes corresponding to E_A.

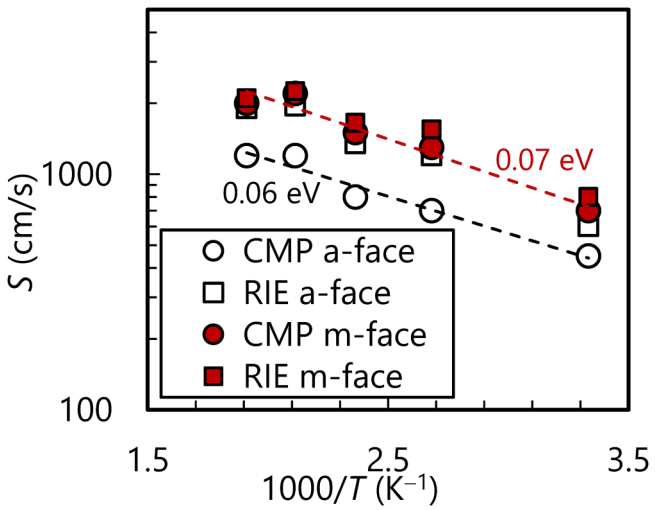

FIG. 5. Temperature dependence of S_a and S_m for the n-type samples, showing a slope E_A of 0.06 eV and 0.07 eV.

350–1550 cm/s for the Si-face and 750–2400 cm/s for the C-face, but seems to be saturated at ~200 °C. From the temperature dependence of S for the CMP-treated surface, we estimate apparent activation energies E_A of 0.1 eV and 0.07 eV for the Si- and C-faces, respectively.

Figure 4 shows the temperature dependence of τ_{epi} for the n-type Si-and C-face samples. Irrespective of the surface treatments, τ_{epi} shows almost the same values. τ_{epi} increases with temperature from 100 °C and reaches 9 μs at 250 °C with E_A of 0.03 eV.

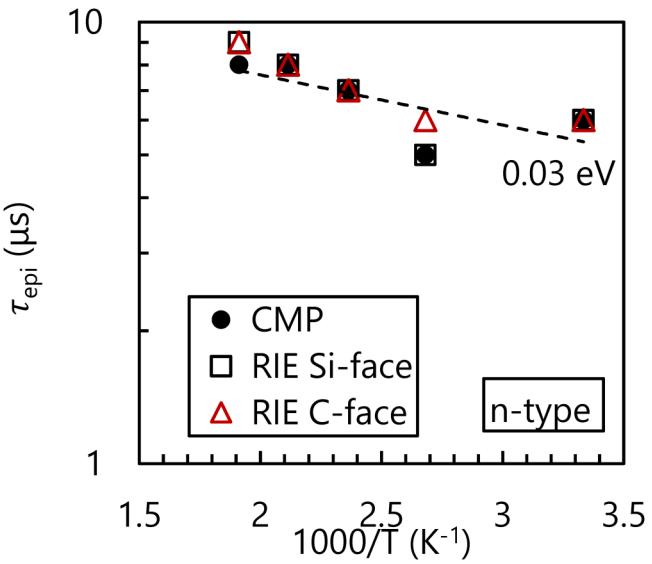

FIG. 4. Temperature dependence of τ_{epi} for the n-type Si and C-face samples.

We performed the same measurements and analyses for the *a*- and *m*-face n-type samples. The estimated S for the *a*-face S_a and for the *m*-face S_m are shown in Fig. 5. For the CMP-treated surfaces, S_a are in the range of 450–1200 cm/s, which are similar values to S_C, whereas S_m are larger than S_a and in the range of 700–2200 cm/s. S_a and S_m for the CMP-treated surfaces monotonically increase with temperature. The estimated E_A are 0.06 and 0.07 eV for S_a and S_m, respectively. S_a for the RIE-treated surfaces are larger than those for the CMP-treated surfaces, whereas S_m for the RIE-treated samples are similar to those for the CMP-treated samples. The temperature dependence of S_a and S_m for the RIE-treated samples is very similar to the case of the Si and C-faces. For the RIE-treated surfaces, S_a are in the range of 600–1950 cm/s, and S_m are in the range of 800–2250 cm/s.

Figure 6 shows the temperature dependence of τ_{epi} for the *a*- and *m*-face samples. As observed in the Si- and C-face samples, RIE treatment does not significantly change τ_{epi}. Compared with τ_{epi} for the Si- and C-face samples, τ_{epi} for the *a*- and *m*-face samples are small and show similar temperature dependence: τ_{epi} increases with temperature with E_A of 0.05–0.06 eV. τ_{epi} for the *a*-face samples (1.2–3.2 μs) are larger than those for the *m*-face samples (0.7–2.1 μs) due to unintentionally high donor doping in the *m*-face samples resulting in higher $Z_{1/2}$ center concentration.[35] We confirmed higher $Z_{1/2}$ center concentrations in the *m*-face samples by using deep level transient spectroscopy (DLTS); the $Z_{1/2}$ center concentrations are 3×10^{13} and 4×10^{14} cm^{-3} for the *a*- and *m*-face samples, whereas in the Si- and C-face samples, it is 5×10^{12} cm^{-3} as in Ref. 21.

For the p-type samples, we also estimated the temperature dependence of S_{Si} and S_C as shown in Fig. 7. As in the n-type samples, S_C are larger than S_{Si}, and S for the RIE-treated surfaces are larger than those for the CMP-treated surfaces. S_{Si} increases with temperature monotonically for the CMP-treated surfaces from 400 cm/s to 1550 cm/s with E_A of 0.08 eV, and S_C shows weaker

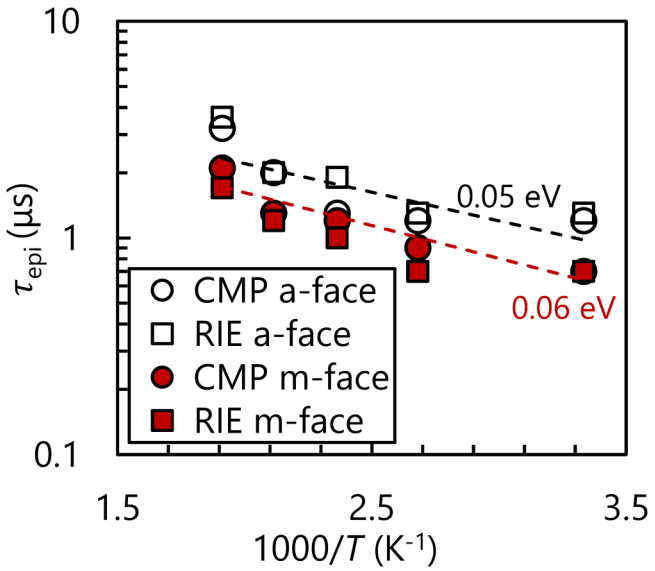

FIG. 6. Temperature dependence of τ_{epi} for the n-type *a*- and *m*-face samples.

temperature dependence and is in the range of 1350–2800 cm/s with an E_A of 0.05 eV. RIE treatment increases S_{Si} but not S_C, and their values are in ranges of 1100–2400 cm/s and 1950–3000 cm/s for S_{Si} and S_C, respectively.

Figure 8 shows the temperature dependence of τ_{epi} for the p-type Si- and C-face samples. τ_{epi} are smaller than the n-type Si- and C-face samples, and surface treatment does not have a significant effect on τ_{epi}. The temperature dependence of τ_{epi} is not remarkable and has a tendency to increase from 150 to 200 °C. τ_{epi} for the p-type samples are in the range of 1.9–3.9 μs. The estimated S and τ_{epi} for all the samples are summarized in Table I.

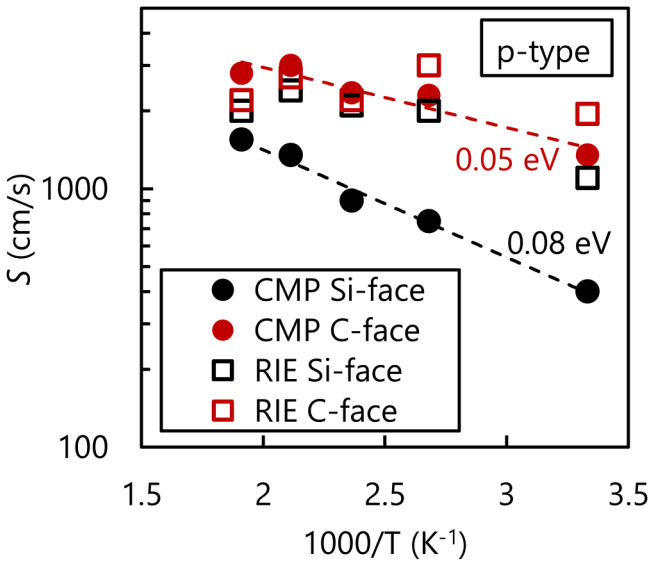

FIG. 7. Temperature dependence of S_{Si} and S_C for the p-type samples.

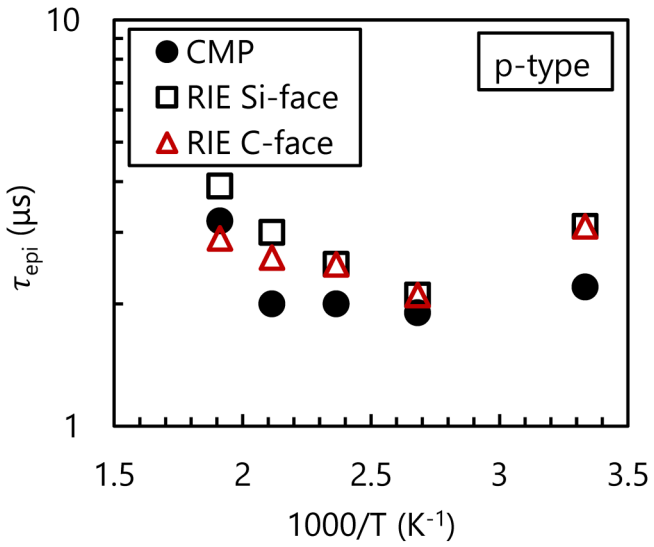

FIG. 8. Temperature dependence of τ_{epi} for the p-type Si- and C-face samples.

DISCUSSION

As for the surface treatment, RIE treatment does not have a significant effect on τ_{epi} for all the samples. This is reasonable and supports the validity of our analysis method, because RIE treatment introduces damage only at the surface of the samples, resulting in the same τ_{epi} irrespective of surface treatment. RIE treatment significantly increases S for the Si- and *a*-faces, whereas for the C- and

TABLE I. Summary of the estimated surface recombination velocities.

Conductivity	Crystal face	τ_{epi} at RT (μs)	τ_{epi} at 250 °C (μs)	Treatment	S at RT (cm/s)	S at 250 °C (cm/s)
n-type	Si-face	6	8–9	CMP	150	800
				RIE	350	1550
	C-face			CMP	500	1500
				RIE	750	2400
	a-face	1.2–1.3	3.2–3.6	CMP	450	1200
				RIE	600	1950
p-type	*m*-face	0.7	1.7–2.1	CMP	700	2200
				RIE	800	2250
	Si-face	2.2–3.1	2.9–3.9	CMP	400	1550
				RIE	1100	2000
	C-face			CMP	1350	2800
				IE	1950	2200

m-faces, which have large *S* even at the CMP-treated surfaces, RIE treatment does not change *S*. This result indicates that the CMP-treated surfaces with large *S* already have a large number of defects acting as surface recombination centers, and thus the effect of the defects induced by the RIE treatment is negligible. For the CMP-treated surfaces for the Si- and *a*-faces, *S* shows monotonic temperature dependence. After the RIE treatment, the dependence becomes weak and is similar for the C- and *m*-faces. This result suggests that RIE introduces a different kind of defects than those at the CMP-treated surfaces of the Si- and *a*-faces.

For the CMP-treated surfaces, considering difference in the *a*- and *m*-face samples, larger *S* are observed for the samples with smaller τ_{epi}. This result implies that defects acting as surface recombination centers at the CMP-treated surfaces interact with the recombination centers in the bulk. Therefore, for example, methods for reduction of the $Z_{1/2}$ center may have secondary effects for the reduction of surface recombination at CMP-treated surfaces,[36,37] if the methods do not induce surface defects such as oxygen related deep levels.[38] On the other hand, S_{Si} of the CMP-treated surfaces are significantly smaller than S_C for both the n- and p-type samples. As previously reported,[23] surface recombination at the Si-face can be passivated by acidic aqueous solutions but not at the C-face. Although we have also tried to passivate surface recombination at the *a*- and *m*-faces by the acidic solutions, only the Si-face can be passivated. This result suggests that dominant recombination centers at the Si-face are different from those at the other crystal faces. A candidate for the centers is surface states from Si dangling bonds, as discussed in Ref. 23.

The p-type samples show larger S_{Si} and S_C than the n-type samples. p-type epilayers typically have a larger number of deep levels and show smaller τ_{epi} as shown in Fig. 8 compared with n-type epilayers. As discussed above, since concentration of the bulk recombination centers seems to have a relationship with concentration of the surface recombination centers, the larger *S* for the p-type SiC possibly comes from the recombination centers in the bulk. On the other hand, the temperature dependence of *S* for the p-type samples is similar to the n-type samples with slightly small E_A.

The temperature dependence of *S* has been discussed by Klein *et al.*[17] Their model is based on the presence of the surface band bending (the space charge region), and thus *S* follows the exponential temperature dependence as

$$S_{eff}(T) = S_\infty e^{\frac{-q\varphi_S}{kT}}, \tag{5}$$

where S_{eff} is the effective surface recombination velocity at the edge of the space charge region, S_0 is the surface recombination velocity just at the surface, *q* is the elementary charge, φ_S is the potential of the surface band bending, and *k* is the Boltzmann constant. S_∞ itself possibly has temperature dependence due to emission or capture of carriers at surface recombination centers, and its temperature dependence may be included in values of E_A in our results. However, by assuming it as constant as in Ref. 17, E_A can be treated as $q\varphi_S$. As described in the previous section, the observed E_A for the CMP-treated surfaces are within 0.05–0.1 eV, which is much smaller than the reported $q\varphi_S$ (0.23–0.28 eV) in Ref. 17. Although the origins of the difference are not clear, the samples in Ref. 17 were thin epilayers (18–35 μm) on the substrate without CMP-treatments. As discussed in Ref. 21, the as-grown surfaces show significant differences in *S* compared with the CMP-treated surfaces, and analyses to thin epilayers include difficulties for the separation of the bulk and surface recombination. These differences may induce different values for the surface band bending. On the other hand, RIE treatment weakens the temperature dependence of *S*. The weak temperature dependence can be interpreted as the small band bending at the surface or presence of the recombination centers at the edge of the space charge region. Therefore, defects induced by RIE distribute within the space charge region affecting the charge concentration or recombination center concentration.

The temperature dependence of τ_{epi} is similar among the n-type samples, although absolute values depend on the crystal faces. This temperature dependence is also similar to the previously reported bulk carrier lifetimes in PiN diodes with and without the $Z_{1/2}$ reduction process: E_A of 0.07 eV.[39] On the other hand, the difference in the absolute values possibly comes from the difference in concentration of recombination centers such as the $Z_{1/2}$ center as observed by DLTS. Considering the similar temperature dependence of τ_{epi} among all the samples including previously reported ones[39] and τ_{epi} dependence on the $Z_{1/2}$ center concentration, the $Z_{1/2}$ center is the dominant bulk recombination center in the n-type SiC, as has been discussed previously.[1] On the other hand, for the p-type samples, the temperature dependence of τ_{epi} is different from those for the n-type samples. The recombination behavior in p-type materials is, of course, different from n-type materials even in the presence of the same recombination center. There would be other recombination centers than the $Z_{1/2}$ center in p-type SiC as discussed in Ref. 14.

The obtained *S* in this study are smaller than previously reported values.[16–27] One of the reasons is our low excitation intensity compared with previous reports. As seen in our recent report (Ref. 23), S_{Si} was evaluated as 800 cm/s, compared with 150 cm/s in this study. The previous one was observed at the excitation photon density of 8×10^{13} cm^{-2}, which is four times larger than the employed intensity in this study. As has been discussed regarding the surface recombination phenomenon for Si, *S* increases with the excitation intensity,[40] and most reported *S* for SiC are observed at higher excitation intensities compared with this study. We are now estimating quantitative *S* dependence on the excitation intensity, and we will report the results in the near future.

CONCLUSIONS

We have determined *S* and τ_{epi} with their temperature dependence for the Si- and C-faces of the n- and p-type 4H-SiC and also for the *a*- and *m*-faces of n-type 4H-SiC by using an improved measurement technique and analysis method. For CMP-treated surfaces, *S* monotonically increases with temperature, and comparing *S* and τ_{epi} among the samples, the concentration of recombination centers at the surfaces appears to be related to the recombination center concentration in the bulk. On the other hand, the Si-face shows the smallest *S* among the crystal faces irrespective of the conductivity type, so there are different recombination centers at the Si-face than the other crystal faces. After

RIE treatment, S increased and had weaker temperature dependence for the samples that had small S for the CMP-treated surfaces, indicating that the defects induced by the RIE treatment act as charged deep levels or recombination centers in the space charge region. We believe that such a comprehensive survey and discussion of quantitative values of S will support future improvements in the design and development of bipolar SiC devices.

ACKNOWLEDGMENTS

The authors thank Professor Kimoto of the Kyoto University for his help in sample preparation and discussion.

DATA AVAILABILITY

The data that support the findings of this study are available from the corresponding author upon reasonable request.

REFERENCES

[1]T. Kimoto and J. A. Cooper, *Fundamentals of Silicon Carbide Technology* (John Wiley & Sons, Singapore, 2014).
[2]M. Bakowski, IEE J. Trans. Ind. Appl. **126**, 391 (2006).
[3]Q. Zhang, M. Das, J. Sumakeris, R. Callanan, and A. Agarwal, IEEE Electron Device Lett. **29**, 1027 (2008).
[4]S. Chowdhury, C. Hitchcock, Z. Stum, R. Dahal, I. B. Bhat, and T. P. Chow, IEEE Electron Device Lett. **37**, 317 (2016).
[5]N. Kaji, H. Niwa, J. Suda, and T. Kimoto, IEEE Trans. Electron Devices **62**, 374 (2015).
[6]H. Miyake, T. Okuda, H. Niwa, T. Kimoto, and J. Suda, IEEE Electron Device Lett. **33**, 1598 (2012).
[7]T. Kimoto and Y. Yonezawa, Mater. Sci. Semicond. Process. **78**, 43 (2018).
[8]P. B. Klein, J. Appl. Phys. **103**, 033702 (2008).
[9]M. Kato, Y. Matsushita, M. Ichimura, T. Hatayama, and T. Ohshima, Jpn. J. Appl. Phys. **51**, 028006 (2012).
[10]P. Ščajev, V. Gudelis, K. Jarašiūnas, and P. B. Klein, J. Appl. Phys. **108**, 023705 (2010).
[11]K. Danno, D. Nakamura, and T. Kimoto, Appl. Phys. Lett. **90**, 202109 (2007).
[12]T. Mori, M. Kato, H. Watanabe, M. Ichimura, E. Arai, S. Sumie, and H. Hashizume, Jpn. J. Appl. Phys. **44**, 8333 (2005).
[13]M. Kato, M. Kawai, T. Mori, M. Ichimura, S. Sumie, and H. Hashizume, Jpn. J. Appl. Phys. **46**, 5057 (2007).
[14]T. Hayashi, K. Asano, J. Suda, and T. Kimoto, J. Appl. Phys. **109**, 014505 (2011).
[15]T. Miyazawa, M. Ito, and H. Tsuchida, Appl. Phys. Lett. **97**, 202106 (2010).
[16]A. Galeckas, J. Linnros, M. Frischholz, and V. Grivckas, Appl. Phys. Lett. **79**, 365 (2001).
[17]P. B. Klein, R. Myers-Ward, K.-K. Lew, B. L. VanMil, C. R. Eddy, Jr., D. K. Gaskill, A. Shrivastava, and T. S. Sudarshan, J. Appl. Phys. **108**, 033713 (2010).
[18]T. Kimoto, T. Hiyoshi, T. Hayashi, and J. Suda, J. Appl. Phys. **108**, 083721 (2010).
[19]T. Kimoto, Y. Nanen, T. Hayashi, and J. Suda, Appl. Phys. Express **3**, 121201 (2010).
[20]T. Okuda, T. Kobayashi, T. Kimoto, and J. Suda, Appl. Phys. Express **9**, 051301 (2016).
[21]M. Kato, A. Yoshida, and M. Ichimura, Jpn. J. Appl. Phys. **51**, 02BP12 (2012).
[22]Y. Mori, M. Kato, and M. Ichimura, J. Phys. D Appl. Phys. **47**, 335102 (2014).
[23]Y. Ichikawa, M. Ichimura, T. Kimoto, and M. Kato, ECS J. Solid State Sci. Technol. **7**, Q127 (2018).
[24]S. S. Suvanam, K. Gulbinas, M. Usman, M. K. Linnarson, D. M. Martin, J. Linnros, V. Grivickas, and A. Hallén, J. Appl. Phys. **117**, 105309 (2015).
[25]S. Asada, J. Suda, and T. Kimoto, IEEE Trans. Electron Devices **65**, 4786 (2018).
[26]K. Nakayama, A. Tanaka, M. Nishimura, K. Asano, T. Miyazawa, M. Ito, and H. Tsuchida, IEEE Trans. Electron Devices **59**, 895 (2012).
[27]T. Asada, Y. Ichikawa, and M. Kato, J. Vis. Exp. **146**, e59007 (2019).
[28]M. Kato, Y. Mori, and M. Ichimura, Jpn. J. Appl. Phys. **54**, 04DP14 (2015).
[29]L. Subačius, K. Jarašiūnas, P. Ščajev, and M. Kato, Meas. Sci. Technol. **26**, 125014 (2015).
[30]M. Kato, S. Katahira, Y. Ichikawa, S. Harada, and T. Kimoto, J. Appl. Phys. **124**, 095702 (2018).
[31]S. G. Sridhara, T. J. Eperjesi, R. P. Devaty, and W. J. Choyke, Mater. Sci. Eng. B **61–62**, 229 (1999).
[32]N. Watanabe, T. Kimoto, and J. Suda, Jpn. J. Appl. Phys. **53**, 108003 (2014).
[33]P. Scajev and K. Jarasiunas, J. Phys. D Appl. Phys. **46**, 265304 (2013).
[34]T. Hayashi, T. Okuda, J. Suda, and T. Kimoto, Jpn. J. Appl. Phys. **53**, 111301 (2014).
[35]I. Pintilie, L. Pintilie, K. Irmscher, and B. Thomas, Appl. Phys. Lett. **81**, 4841 (2002).
[36]L. Storasta, F. H. C. Carlsson, J. P. Bergman, and E. Janzén, Appl. Phys. Lett. **86**, 091903 (2005).
[37]T. Hiyoshi and T. Kimoto, Appl. Phys. Express **2**, 041101 (2009).
[38]K. Kawahara, J. Suda, and T. Kimoto, Appl. Phys. Express **6**, 051301 (2013).
[39]A. Tanaka, K. Nakayama, K. Asano, T. Miyazawa, and H. Tsuchida, Jpn. J. Appl. Phys. **53**, 04EP08 (2014).
[40]S. W. Glunz, A. B. Sproul, W. Warta, and W. Wettling, J. Appl. Phys. **75**, 1611 (1994).